J. Fluid Mech. (2008), *vol.* 610, *pp.* 391–406. © 2008 Cambridge University Press
doi:10.1017/S0022112008002577 Printed in the United Kingdom

Linear instability of annular Poiseuille flow

C. J. HEATON

Department of Applied Mathematics and Theoretical Physics, University of Cambridge, Wilberforce Road, Cambridge CB3 0WA, UK

(Received 29 February 2008 and in revised form 22 May 2008)

The linear stability of flow along an annular pipe formed by two coaxial circular cylinders is considered. We find that the flow is unstable above a critical Reynolds number for all $0 < \eta \leqslant 1$, where η is the ratio between the radii of the inner and outer cylinders. This contradicts a recent claim that the flow is stable at all Reynolds numbers for radius ratio η less than a finite critical value. We find that non-axisymmetric disturbances become stable at all Reynolds numbers for $\eta < 0.11686215$, and we are able to study this 'bifurcation from infinity' asymptotically. However, axisymmetric disturbances remain unstable, with critical Reynolds number tending to infinity as $\eta \to 0$. A second asymptotic analysis is performed to show that the critical Reynolds number $Re_c \propto \eta^{-1} \log(\eta^{-1})$ as $\eta \to 0$, with the form of the mean flow profile causing the appearance of the logarithm. The stability of Hagen–Poiseuille flow ($\eta = 0$) at all Reynolds numbers is therefore interpreted as a limit result, and there are no annular pipe flows which share this stability.

1. Introduction

Annular Poiseuille flow (APF), the flow between two coaxial circular cylinders driven by an axial pressure gradient, provides an interesting problem in hydrodynamic stability theory and has been studied or discussed several times over the years (Mott & Joseph 1968; Mahadevan & Lilley 1977; Garg 1980; Landau & Lifshitz 1987; Cotrell & Pearlstein 2006). APF is a special case of 'thread–annular flow', a flow with medical applications, and some results on APF stability can also be found in this context (see Walton 2005, and references therein). In addition to the basic wish to understand the properties of APF, a further reason for the interest in APF is that the narrow-gap limit of APF recovers plane Poiseuille flow, whereas the wide-gap limit recovers Hagen–Poiseuille flow (HPF), so APF connects these two important canonical flows. The relation to HPF provides some additional motivation for investigating the stability of APF, which is the main subject of this paper. We note that several previous studies have given rational asymptotic insight into HPF stability using various different approaches. These include studies of entry flow in a circular pipe (Smith & Bodonyi 1980), flow in non-circular pipes (Smith 1979*a*, *b*; Davey & Salwen 1994; Kerswell & Davey 1996) and nonlinear stability theory (Smith & Bodonyi 1982).

Mott & Joseph (1968) considered axisymmetric disturbances to APF and found these disturbances to be linearly unstable. They computed the critical Reynolds number Re_c for axisymmetric instability in the range $0.3 \leqslant \eta \leqslant 1$, where η is the ratio of the radii of the inner and outer cylinders. Mott & Joseph's critical Reynolds number increases monotonically between $\eta = 1$ (the plane Poiseuille-flow limit) and $\eta = 0.3$, and they conjecture that it will continue to increase, and indeed blow up, as

https://doi.org/10.1017/S0022112008002577 Published online by Cambridge University Press

$\eta \to 0$ (the HPF limit). Mott & Joseph thus conclude that 'the absolute stability of Hagen–Poiseuille flow is evidently a limit result'. Landau & Lifshitz (1987, § 28) come to a similar conclusion, although they do not present detailed arguments. Whether the stability of HPF is recovered in this way as a limit result of APF as $\eta \to 0$ is uncertain for two reasons. (i) Mott & Joseph's conjecture is extrapolated from fairly limited data ($0.3 \leqslant \eta \leqslant 1$). (ii) Since there is no analogue of Squire's theorem in the cylindrical geometry of APF, non-axisymmetric disturbances must also be considered.

Non-axisymmetric stability computations were first performed by Mahadevan & Lilley (1977) and Garg (1980), who both found that the non-axisymmetric disturbances are more unstable than the axisymmetric ones for small η. As part of a study of the topology of the neutral curves of spiral Poiseuille flow, Cotrell & Pearlstein (2006) have given further APF calculations confirming this. Cotrell & Pearlstein's data extend down to $\eta = 0.12$, for which the critical Reynolds number $Re_c = 205\,486$; this is the smallest value of η and the largest value of Re_c to date. For η less than approximately 0.4, Cotrell & Pearlstein find that disturbances with azimuthal order $m = 1$ are the most unstable, and that Re_c increases rapidly for decreasing η. Further, Cotrell & Pearlstein (2006) conclude from their data that Re_c will blow up to infinity at a finite value $\eta \simeq 0.115$, and that for η smaller than this value, APF is absolutely stable at all Re. This conclusion disagrees with the 'limit result' conclusion of Mott & Joseph. If true, Cotrell & Pearlstein's conclusion implies an extended class of annular pipe flows which are absolutely stable (i.e. stable for all azimuthal orders), and that HPF can be viewed as one member of this class.

The motivation for the present paper is therefore to investigate the conclusions of Mott & Joseph (1968) and Cotrell & Pearlstein (2006) using asymptotic arguments. If Re_c blows up as $\eta \to 0$, as asserted by Mott & Joseph, then we might hope to confirm it by describing the process asymptotically. If instead, Re_c blows up at a finite value of $\eta \simeq 0.115$, as asserted by Cotrell & Pearlstein, then we might hope to confirm this by asymptotic arguments. In addition, we shall give further numerical calculations, which extend to smaller η and larger Re than the previously published data, with which to compare and assess the asymptotic results.

We find that the non-axisymmetric disturbances do become stable at all Re for η less than a finite critical value, approximately equal to the value found by Cotrell & Pearlstein (2006). This process occurs as a 'bifurcation from infinity' at the critical value of η and closely follows the behaviour found by Cowley & Smith (1985), who studied the stability of flow intermediate between plane Poiseuille and plane Couette flows. An asymptotic analysis for η close to criticality near the bifurcation point is possible, and we find that this quantitatively recovers the results for Re_c obtained in our numerical calculations. However, axisymmetric disturbances do not possess this bifurcation, and instead our numerical calculations indicate that they remain unstable with $Re_c \to \infty$ as $\eta \to 0$. This is confirmed by a second asymptotic analysis performed for η close to zero, which again is able to quantitatively recover the numerical results. The good agreement between our asymptotic and numerical results suggests that a correct description of the APF stability properties is obtained. We infer that Cotrell & Pearlstein's conclusion is incorrect, and that, in fact, APF is unstable above a critical Reynolds number for all non-zero η, in agreement with Mott & Joseph's conclusion.

The remainder of this paper is organized as follows. In § 2, we give the governing equations and present the results of our numerical stability computations. In § 3, we consider non-axisymmetric disturbances and give the asymptotic description of the blow-up of Re_c at finite η. In § 4, we give an alternative asymptotic treatment for axisymmetric disturbances in the limit $\eta \to 0$. Finally, the results are discussed in § 5.

https://doi.org/10.1017/S0022112008002577 Published online by Cambridge University Press

2. Governing equations and numerical calculations

2.1. *Problem formulation*

Incompressible fluid is confined between two coaxial circular cylinders and driven by a constant axial pressure gradient. The problem is non-dimensionalized by scaling lengths with the gap width, scaling velocities with the averaged axial velocity, and scaling densities with the constant fluid density.

Working in cylindrical polar coordinates (x, r, θ) aligned with the axis of the cylinders, the steady mean flow is APF and is given by

$$U(r) = 2\frac{(1-r^2(1-\eta)^2)\log\eta - (1-\eta^2)\log(r(1-\eta))}{1-\eta^2+(1+\eta^2)\log\eta} \tag{2.1}$$

for

$$\frac{\eta}{1-\eta} \leqslant r \leqslant \frac{1}{1-\eta}, \tag{2.2}$$

where $\eta < 1$ is the radius ratio of the cylinders.

The linear stability equations are obtained by introducing a small disturbance velocity $(u, v, w)\mathrm{e}^{\mathrm{i}m\theta+\mathrm{i}kx-\mathrm{i}\omega t}$ and disturbance pressure $p\mathrm{e}^{\mathrm{i}m\theta+\mathrm{i}kx-\mathrm{i}\omega t}$. The wavenumbers m and k are assumed real, with m an integer, and the complex amplitudes u, v, w and p are functions of radius r. The linearized Navier–Stokes equations become

$$\mathrm{i}(Uk-\omega)u + vU' = -\mathrm{i}kp + Re^{-1}\left[u'' + \frac{u'}{r} - \left(\frac{m^2}{r^2}+k^2\right)u\right], \tag{2.3}$$

$$\mathrm{i}(Uk-\omega)v = -p' + Re^{-1}\left[v'' + \frac{v'}{r} - \left(\frac{1+m^2}{r^2}+k^2\right)v - \frac{2\mathrm{i}mw}{r^2}\right], \tag{2.4}$$

$$\mathrm{i}(Uk-\omega)w = -\frac{\mathrm{i}mp}{r} + Re^{-1}\left[w'' + \frac{w'}{r} - \left(\frac{1+m^2}{r^2}+k^2\right)w + \frac{2\mathrm{i}mv}{r^2}\right], \tag{2.5}$$

$$0 = \mathrm{i}ku + v' + \frac{v}{r} + \frac{\mathrm{i}mw}{r}, \tag{2.6}$$

where prime denotes differentiation with respect to r and Re is the Reynolds number based on the average axial flow. The boundary conditions for the disturbance are no slip on the two cylinders,

$$u = v = w = 0 \quad \text{at} \quad r = \eta/(1-\eta), \quad 1/(1-\eta). \tag{2.7}$$

Equations (2.3)–(2.7) define the eigenvalue problem for the complex frequency ω. For a given pair (η, Re), the flow is said to be unstable if there exist k, m such that there is an eigenvalue with $\mathrm{Im}(\omega) > 0$. As mentioned in § 1, there is no analogue of Squire's theorem available for (2.3)–(2.6), so all values of m and k must be considered. The only available simplification is that we may restrict ourselves to $m \geqslant 0$ and $k \geqslant 0$ by making use of the symmetry properties of (2.3)–(2.6).

Before proceeding to the numerical solution, we note that the system (2.3)–(2.6) constitutes a sixth-order system. The system is somewhat similar to the stability equations for planar flows, but it cannot, in general, be simplified into two decoupled equations in the manner of the Orr–Sommerfeld and Squire equations for planar flows (Burridge & Drazin 1969; Drazin & Reid 1981; Schmid & Henningson 2001). For large Re, it is possible to derive six linearly independent asymptotic solutions of (2.3)–(2.6) in the traditional manner: two of inviscid type and four of viscous (dominant-recessive) type. Two of the viscous solutions have the scalings $(u, v, w, p) \propto (1, Re^{-1/2}, Re^{-1}, Re^{-3/2})$, and the other two have the scalings

https://doi.org/10.1017/S0022112008002577 Published online by Cambridge University Press

$(u, v, w, p) \propto (1, Re^{-1/2}, 1, Re^{-3/2})$. The six solutions can be derived using these scalings in the standard way (Drazin & Reid 1981), and can be combined to form various heuristic approximations for large-Re solutions of (2.3)–(2.6), as described by Drazin & Reid (1981, § 27). We mention this for completeness, but in this paper we shall not use these methods of approximation so no further details are given here.

Although we must consider all $m \geqslant 0$, the axisymmetric case $m = 0$ deserves some special mention. When $m = 0$, the system (2.3)–(2.6) can be simplified into a fourth-order system and an uncoupled second-order system similar to the Orr–Sommerfeld and Squire equations. The governing equation analogous to the Orr–Sommerfeld equation is given by Corcos & Sellars (1959) as

$$(Uk - \omega)\left(\phi'' - \frac{\phi'}{r} - k^2\phi\right) + \phi k\left(\frac{U'}{r} - U''\right) = \frac{-\mathrm{i}}{Re}\left[\phi^{\mathrm{iv}} - \frac{2}{r}\phi''' + \frac{3}{r^2}\phi'' - \frac{3}{r^3}\phi' - 2k^2\left\{\phi'' - \frac{\phi'}{r}\right\} + k^4\phi\right], \quad (2.8)$$

where ϕ is the streamfunction for a non-swirling disturbance:

$$u = r^{-1}\phi'(r)\mathrm{e}^{\mathrm{i}kx - \mathrm{i}\omega t}, \quad v = -\mathrm{i}kr^{-1}\phi(r)\mathrm{e}^{\mathrm{i}kx - \mathrm{i}\omega t}, \quad w = 0. \quad (2.9)$$

Therefore, the boundary conditions for (2.8) are

$$\phi = \phi' = 0 \ \text{ at } \ r = \eta/(1-\eta),\ 1/(1-\eta). \quad (2.10)$$

For studying axisymmetric instabilities, the system (2.8)–(2.10) is completely equivalent to the system (2.3)–(2.7) with m set equal to 0. We shall use (2.8)–(2.10) in what follows because using the single fourth-order equation simplifies the asymptotic analysis and also it is easier to compute numerically, making calculations possible at smaller η and larger Re than are possible using the sixth-order formulation.

2.2. *Numerical calculations*

The equations (2.3)–(2.6) and (2.8) are discretized with a pseudospectral collocation method, with the unknown functions represented by Chebyshev polynomials on a Gauss–Lobatto grid. Using N collocation points, (2.3)–(2.6) are transformed into a $(4N \times 4N)$ matrix equation, whereas (2.8) becomes an $(N \times N)$ matrix equation. A generalized eigenvalue problem is solved to determine the eigenvalues ω for given η, Re, k, m. The eigenvalue ω with the greatest imaginary part is the primary eigenvalue, the flow being unstable if its imaginary part is positive. We use MATLAB™ to perform the linear algebra on a standard desktop computer. The generalized eigenvalue calculation has $O(N^3)$ complexity, and typical values of N used were 50 or 100. For cases with larger Re, we found that larger N are required for convergence.

The numerical code is validated by comparison to the results in Cotrell & Pearlstein (2006, table 1), and excellent agreement is found in each case. As a consistency check for the cases with $m = 0$, results obtained from (2.8) were compared with results from (2.3)–(2.6) and the two were found to agree with each other, as well as with the $m = 0$ data in Cotrell & Pearlstein (2006, table 1).

The spectral code described gives the temporal growth rate of the least damped eigenmode, and we now use this to locate and track the neutral curve and critical Reynolds number Re_c. We consider each value of $m = 0, 1, 2, 3, \ldots$ separately in turn. For each m, we begin the calculation by choosing an initial value of η and then using a bisection method to locate a pair (Re, k) for which the least damped mode is neutrally stable. We then use a curve-tracking routine to trace out the entire neutral

https://doi.org/10.1017/S0022112008002577 Published online by Cambridge University Press

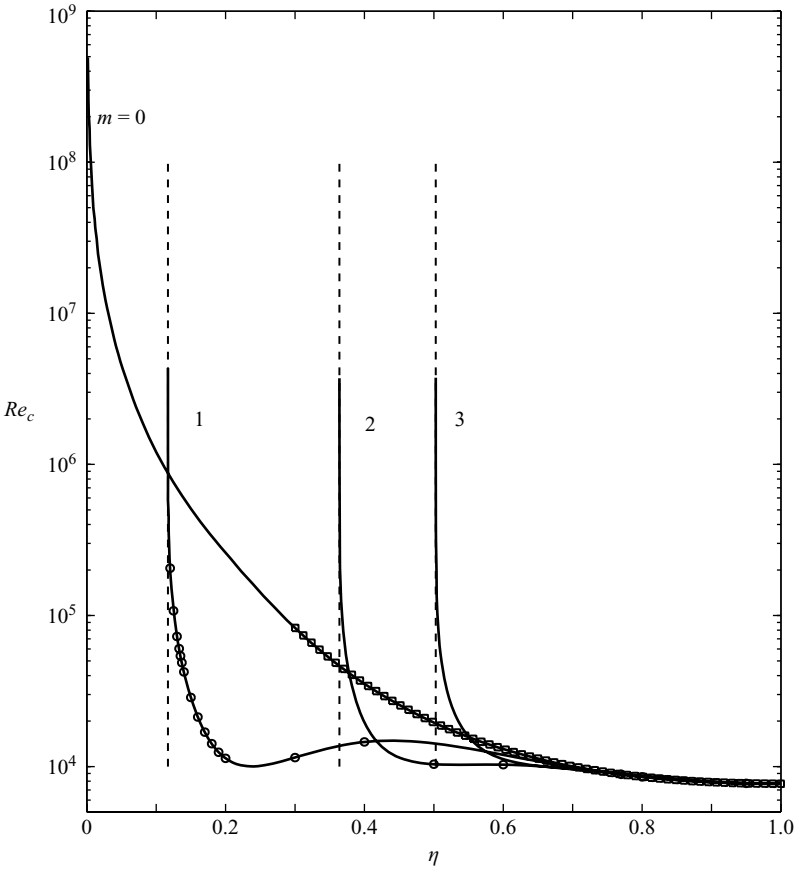


FIGURE 1. The critical Reynolds number Re_c versus radius ratio η for $m = 0, 1, 2, 3$ (solid lines). □, $m = 0$ data from Mott & Joseph (1968, figure 2); ○, data from Cotrell & Pearlstein (2006, table 1). The dashed lines are vertical asymptotes derived in § 3.

curve in the (Re, k)-plane for the given values of m and η. The minimum value of Re on this neutral curve is found by interpolation, and this is the critical Reynolds number Re_c for the given values of m and η. To compute a value of Re_c in this manner is cumbersome and requires many solutions of the eigenvalue problem, but the whole procedure need not be repeated. Instead, a small increment is made to the value of η and a section of the neutral curve near to Re_c is traced out in the (Re, k)-plane for the new value of η, using the data from the previous step as an initial guess. This process is much quicker and can be repeated many times, giving the variation of Re_c and k_c (the critical axial wavenumber) with respect to η.

The results of the numerical calculations are given in figure 1, which shows Re_c plotted against η for $m = 0$, 1, 2 and 3. Both the $m = 0$ data from Mott & Joseph (1968, figure 2) and the data from Cotrell & Pearlstein (2006, table 1) are also plotted in figure 1, to show that our numerical results are consistent with these earlier results. In the limit $\eta \to 1$, the mean flow uniformly approaches plane Poiseuille flow and the minimum critical Reynolds number tends to the value for plane Poiseuille flow (which is $5772 \times 4/3 = 7696$ here, owing to the scalings taken). The behaviour at smaller η is of more interest, however. There is a wide range of η for which the non-axisymmetric modes are much more unstable than the axisymmetric mode. In this range, figure 1

https://doi.org/10.1017/S0022112008002577 Published online by Cambridge University Press

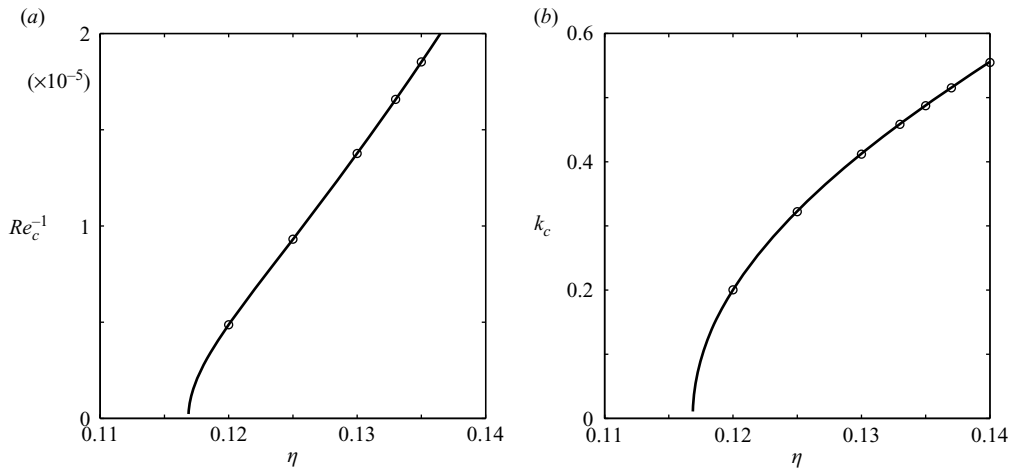


FIGURE 2. For the $m = 1$ modes, variation of (a) critical Reynolds number, (b) critical axial wavenumber. ○, data points from Cotrell & Pearlstein (2006, table 1).

closely resembles figure 4 of Mahadevan & Lilley (1977) and figure 9 of Garg (1980), both of which are restricted to the range $0.15 \leqslant \eta \leqslant 1$. Continuing to smaller η, we find that the axisymmetric mode again becomes the most unstable for $\eta < 0.117$. In the limit $\eta \to 0$, the axisymmetric mode remains the most unstable, and it appears that $Re_c \to \infty$ as $\eta \to 0$.

The results of figure 1 therefore seem to contradict the conclusion of Cotrell & Pearlstein (2006) that APF is stable at all Re for η less than a critical value of approximately 0.115. Instead, figure 1 tends to support the conclusion of Mott & Joseph (1968) that $Re_c \to \infty$ as $\eta \to 0$. Figure 2 suggests that the $m = 1$ modes do have $Re_c \to \infty$ at a finite value of η, in agreement with the finding of Cotrell & Pearlstein (2006), although because of the axisymmetric instability mode, it does not follow that APF is absolutely stable for smaller η.

The numerical evidence of this section indicates that the $m = 1$ modes, and indeed the other non-axisymmetric modes, become stabilized at finite critical values of η. In the following section, we confirm this behaviour by performing an asymptotic analysis. In § 4, we will investigate the $m = 0$ modes as $\eta \to 0$, and confirm the suggestion that $Re_c \to \infty$ in this limit, by performing a different asymptotic analysis.

3. Asymptotics for non-axisymmetric disturbances

Figure 2 strongly suggests that the $m = 1$ modes possess a bifurcation in which $Re_c \to \infty$ and $k_c \to 0$ at a finite value of η, and we now proceed to analyse this process. Similar behaviour is found for the other non-axisymmetric modes with $m = 2, 3, \ldots$, but we shall concentrate on $m = 1$ for this presentation. The starting point for the analysis is found in figure 3, which shows the neutral curve in the (Re, k)-plane for two values of η near to the bifurcation, unstable modes existing in the narrow region enclosed by the neutral curve. The striking feature of figure 3 is that both upper and lower branches of the neutral curve clearly display the same scaling $k \propto Re^{-1}$ for large Re. On investigating the neutral curves, we find that as η decreases, the two asymptotes of the upper and lower branches move closer together and the critical Reynolds number increases. The bifurcation is identified with a radius ratio η^* for which the asymptotes of the upper and lower branches become coincident, and the

https://doi.org/10.1017/S0022112008002577 Published online by Cambridge University Press

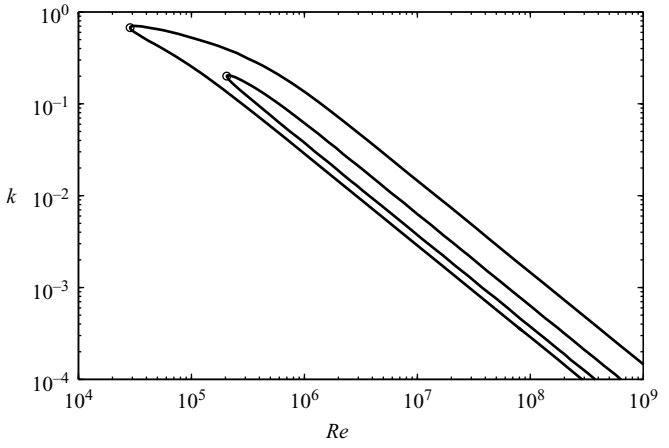


FIGURE 3. The neutral curves for $m=1$ and $\eta=0.15, 0.12$. For each case, a circle shows the critical Reynolds number and axial wavenumber from Cotrell & Pearlstein (2006, table 1).

unstable region between them vanishes. This process is termed a bifurcation from infinity, and is essentially the same as that studied by Cowley & Smith (1985) for a different flow.

To determine η^* we must first determine the location of the upper and lower branch asymptotes as seen in figure 3. The scalings which we observe numerically on the asymptotes are

$$\left.\begin{aligned} &kRe = \lambda_0^{-1}, \\ &\omega = c_0 k, \\ &(u(r), v(r), w(r), p(r)) = (u_0(r), kv_0(r), kw_0(r), k^2 p_0(r)), \end{aligned}\right\} \tag{3.1}$$

where each quantity with a subscript is $O(1)$ as $Re \to \infty$. With these long-wave scalings, (2.3)–(2.6) reduce at leading order to

$$\frac{\mathrm{i}}{\lambda_0}(U-c_0)u_0 + \frac{U'v_0}{\lambda_0} = u_0'' + \frac{u_0'}{r} - \frac{m^2 u_0}{r^2}, \tag{3.2}$$

$$\frac{\mathrm{i}}{\lambda_0}(U-c_0)v_0 = -\frac{p_0'}{\lambda_0} + v_0'' + \frac{v_0'}{r} - \frac{(1+m^2)v_0}{r^2} - \frac{2\mathrm{i}mw_0}{r^2}, \tag{3.3}$$

$$\frac{\mathrm{i}}{\lambda_0}(U-c_0)w_0 = -\frac{\mathrm{i}mp_0}{r\lambda_0} + w_0'' + \frac{w_0'}{r} - \frac{(1+m^2)w_0}{r^2} + \frac{2\mathrm{i}mv_0}{r^2}, \tag{3.4}$$

$$0 = \mathrm{i}u_0 + v_0' + \frac{v_0'}{r} + \frac{\mathrm{i}mw_0}{r}. \tag{3.5}$$

The system (3.2)–(3.5) is a long-wave version of (2.3)–(2.6), with the same no-slip boundary conditions:

$$u_0 = v_0 = w_0 = 0 \quad \text{at} \quad r = \eta/(1-\eta),\ 1/(1-\eta). \tag{3.6}$$

Equations (3.2)–(3.6) are a new eigenvalue problem, the eigenvalue for c_0 being a function of λ_0, η and m. This eigenvalue problem can be solved numerically using the same method as described in § 2 for the solution of (2.3)–(2.7). The neutral curve for this eigenvalue problem, on which $\max\{\mathrm{Im}(c_0)\}=0$, is shown in figure 4 for $m=1$. For both $\eta=0.12$ and 0.15, it can be seen that there are two possible values of λ_0, corresponding to the upper and lower branch asymptotes.

https://doi.org/10.1017/S0022112008002577 Published online by Cambridge University Press

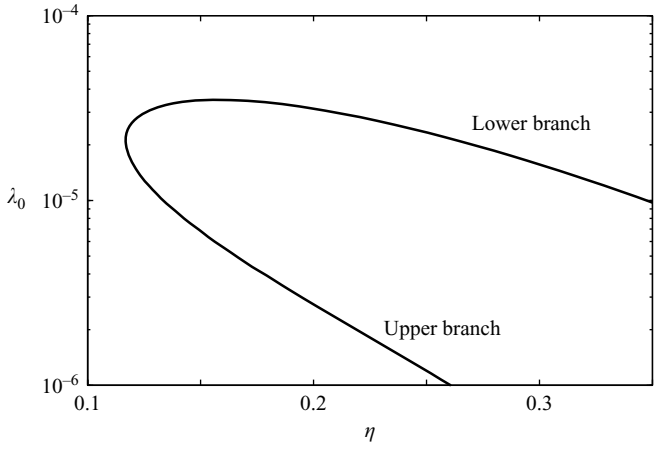


FIGURE 4. The neutral curve of the long-wave equations (3.2)–(3.6) for $m = 1$. The leftmost point on the curve is $\eta = \eta^* = 0.11686215$, $\lambda_0 = 2.1122 \times 10^{-5}$, with $c_0 = 2.7794 \times 10^{-1}$.

For $\eta = 0.12$, we find $\lambda_0 = 1.58 \times 10^{-5}, 2.66 \times 10^{-5}$, whereas for $\eta = 0.15$, we find $\lambda_0 = 6.83 \times 10^{-6}, 3.48 \times 10^{-5}$. All these values are in good agreement with the numerically calculated asymptotes in figure 3. As η decreases, figure 4 shows that the two asymptotes move closer together until for $\eta = \eta^* = 0.11686215$ they coincide, meaning that no unstable region is left in the (Re, k)-plane. The value of η^* derived from figure 4 is shown by a vertical asymptote in figure 1, as are values for $m = 2, 3$ obtained in the same way.

Following Cowley & Smith (1985), now that η^* is known, it is possible to proceed and study the bifurcation asymptotically for $0 < \eta - \eta^* \ll 1$. It is convenient to introduce the small parameter $\delta \ll 1$ such that

$$\eta = \eta^* + \delta^2. \tag{3.7}$$

This is motivated by the fact that a linear change in λ_0 near to the turning point in figure 4 implies a quadratic change to η. A similar argument holds in the (η, c_0)-plane, so we write

$$\lambda = \lambda_0 + \delta\lambda_1 + \delta^2\lambda_2 + \cdots, \tag{3.8}$$

$$c = c_0 + \delta c_1 + \delta^2 c_2 + \cdots. \tag{3.9}$$

The appropriate wavenumber scaling is found from re-plotting the data of figure 2(b) on a log–log scale to be

$$k = \delta k_s. \tag{3.10}$$

The spatial scale and the fast time scale are now determined via k and c, so it only remains to fix the slow time scale, to account for the slow growth or decay of disturbance amplitude. Sandwiched in the narrow gap between two branches of the neutral curve, as shown in figure 3, the disturbance growth rate will be $O((\lambda - \lambda_0)^2)$ slower than the fast time. Hence the time and space scales are:

$$\left.\begin{array}{ll} \tau = \delta k_s c t & \text{fast time,} \\ T = \delta^3 k_s t & \text{slow time,} \\ X = \delta k_s x & \text{space.} \end{array}\right\} \tag{3.11}$$

https://doi.org/10.1017/S0022112008002577 Published online by Cambridge University Press

The scalings of the various quantities all take the same form as for the planar Poiseuille–Couette flow studied by Cowley & Smith (1985), so the analysis proceeds in a very similar fashion. The most significant difference is that the system (2.3)–(2.6) has four dependent variables and leads to more complicated algebra than the Orr–Sommerfeld equation studied by Cowley & Smith (1985).

For consistency with (3.1), we write the dependent variables as

$$\boldsymbol{q} = \begin{pmatrix} u \\ (\delta k_s)^{-1} v \\ (\delta k_s)^{-1} w \\ (\delta k_s)^{-2} p \end{pmatrix} = \boldsymbol{q}_0 + \delta \boldsymbol{q}_1 + \delta^2 \boldsymbol{q}_2 + \cdots, \tag{3.12}$$

and for convenience we shall use the independent variable

$$y = r - \eta/(1-\eta). \tag{3.13}$$

Using y instead of r means that the domain of the problem is $0 \leqslant y \leqslant 1$ and is independent of η, which will simplify the definition of the inner product to follow.

The governing equations (2.3)–(2.6) are expanded for small δ as

$$(L_0 + \delta L_1 + \delta^2 L_2 + \cdots)(\boldsymbol{q}_0 + \delta \boldsymbol{q}_1 + \delta^2 \boldsymbol{q}_2 + \cdots) = 0, \tag{3.14}$$

giving a sequence of problems

$$L_0 \boldsymbol{q}_0 = 0, \tag{3.15}$$

$$L_0 \boldsymbol{q}_1 = -L_1 \boldsymbol{q}_0, \tag{3.16}$$

$$L_0 \boldsymbol{q}_2 = -L_1 \boldsymbol{q}_1 - L_2 \boldsymbol{q}_0, \tag{3.17}$$

$$\vdots$$

where the operators L_0, L_1 and L_2 are given in the Appendix.

We restrict attention to solutions which are 2π-periodic in both X and τ. Assuming $\boldsymbol{q}_0 \propto a(T)\mathrm{e}^{\mathrm{i}(X-\tau)}$, (3.15) is equivalent to (3.2)–(3.5), so λ_0 and c_0 take the values already determined from the leading-order problem and given in the caption of figure 4.

Equation (3.16) requires a solvability condition to be satisfied, so we now define an inner product by

$$\langle \boldsymbol{q}_a, \boldsymbol{q}_b \rangle = \int_0^{2\pi} \mathrm{d}X \int_0^{2\pi} \mathrm{d}\tau \int_0^1 \mathrm{d}y\, \overline{\boldsymbol{q}_a}^t \boldsymbol{q}_b. \tag{3.18}$$

From (3.16) the solvability condition for $\boldsymbol{q}_1$ is

$$\langle \boldsymbol{q}_0^+, L_1 \boldsymbol{q}_0 \rangle = 0, \tag{3.19}$$

where $\boldsymbol{q}_0^+$ denotes the eigenfunction of L_0^+, the adjoint operator with respect to our inner product (3.18). Now, since λ_0 and c_0 are known, from (A 3) we can write

$$L_1 = \lambda_1 M_1 + c_1 M_2 \tag{3.20}$$

for known operators M_1, M_2. The solvability condition (3.19) then becomes

$$c_1 = f\lambda_1 \text{ for } f \equiv -\langle \boldsymbol{q}_0^+, M_1 \boldsymbol{q}_0 \rangle / \langle \boldsymbol{q}_0^+, M_2 \boldsymbol{q}_0 \rangle. \tag{3.21}$$

Since we wish the fast time variable τ to describe harmonic variation of $\boldsymbol{q}$ but not slow growth of the amplitude (which is governed by the slow time T), all the coefficients c_i in (3.9) must be real. As a consequence $f = c_1/\lambda_1$ is necessarily a real quantity. With the solvability condition satisfied, the solution of (3.16) is

$$\boldsymbol{q}_1 = \lambda_1 \boldsymbol{Q}_1 \quad \text{for} \quad L_0 \boldsymbol{Q}_1 = (-M_1 - f M_2)\boldsymbol{q}_0. \tag{3.22}$$

https://doi.org/10.1017/S0022112008002577 Published online by Cambridge University Press

Note that $\boldsymbol{Q}_1$ is derived from known quantities and so is calculable, but λ_1 and $\boldsymbol{q}_1$ are still undetermined.

From (3.17), the solvability condition for $\boldsymbol{q}_2$ is

$$\langle \boldsymbol{q}_0^+, L_1\boldsymbol{q}_1 + L_2\boldsymbol{q}_0\rangle = 0. \tag{3.23}$$

Now we use (A 4) to write

$$L_2 = -\lambda_0^{-1}\left(\lambda_1^2 - \lambda_0\lambda_2\right)M_1 + \left[\mathrm{i}(\lambda_0^{-1}\lambda_1 c_1 - c_2) + \partial_T\right]\mathrm{i}M_2 + k_s^2 M_3 + M_4, \tag{3.24}$$

where M_1, M_2 are as before and M_3, M_4 are two more known operators. After some algebraic manipulations, which are omitted for brevity, the solvability condition (3.23) yields the following condition on the slow growth of the amplitude:

$$Re\left(\frac{1}{a}\frac{\partial a}{\partial T}\right) = \lambda_1^2 Re\left(\frac{\mathrm{i}\langle \boldsymbol{q}_0^+, (M_1 + fM_2)\boldsymbol{Q}_1\rangle}{\langle \boldsymbol{q}_0^+, M_2\boldsymbol{q}_0\rangle}\right) + k_s^2 Re\left(\frac{\mathrm{i}\langle \boldsymbol{q}_0^+, M_3\boldsymbol{q}_0\rangle}{\langle \boldsymbol{q}_0^+, M_2\boldsymbol{q}_0\rangle}\right) + Re\left(\frac{\mathrm{i}\langle \boldsymbol{q}_0^+, M_4\boldsymbol{q}_0\rangle}{\langle \boldsymbol{q}_0^+, M_2\boldsymbol{q}_0\rangle}\right) \tag{3.25}$$

$$= \lambda_1^2\mu_1 + k_s^2\mu_2 + \mu_3. \tag{3.26}$$

The μ_1, μ_2, μ_3 are given in terms of determined quantities, and so are calculable. Setting the left-hand side of (3.26) to zero gives the asymptotic location of the neutral curve, and by using (3.7)–(3.10) to eliminate λ_1 and k_s in favour of η and Re gives the formulae for the critical Reynolds number and axial wavenumber:

$$Re_c = (k_c\lambda_0)^{-1}, \tag{3.27}$$

$$k_c^2 = -\mu_2^{-1}\mu_3(\eta - \eta^*). \tag{3.28}$$

The coefficients μ_1, μ_2, μ_3 in (3.26) are computed as follows. First, the values of η^*, λ_0 and c_0 are determined from the leading-order problem (3.2)–(3.5) (or equivalently (3.15)), as in figure 4. The corresponding neutrally stable eigenfunction of L_0 is $\boldsymbol{q}_0$. The adjoint operator L_0^+ can be derived in the standard manner, so the corresponding adjoint eigenfunction $\boldsymbol{q}_0^+$ can also be computed. With knowledge of the numerical values of η^*, λ_0 and c_0, all of the operators M_i in (3.21), (3.22) and (3.25) are known, and so it is possible to compute, in turn, f, $\boldsymbol{Q}_1$ and the μ_i. We find

$$\mu_1 = -1.529 \times 10^7, \quad \mu_2 = -1.138 \times 10^{-2}, \quad \mu_3 = 1.500 \times 10^{-1}. \tag{3.29}$$

The asymptotic predictions (3.27),(3.28) based on these values are shown by dashed lines in figure 5. The agreement with the numerical data is very good, so we conclude that the analysis of this section gives a correct description of the bifurcation for non-axisymmetric disturbances in APF.

4. Asymptotics for axisymmetric disturbances

The numerical data in figure 1 suggested that the $m = 0$ modes have a critical Reynolds number $Re_c \to \infty$ in the limit $\eta \to 0$. A closer inspection of the data on log–log plots reinforces this (see the solid lines on figure 7). It is evident from figure 7 that the scaling of Re_c with η is different from the scaling (3.27) for $m \neq 0$, so the bifurcation studied in § 3 is not present here. This is further confirmed by inspecting some neutral curves in the (Re, k)-plane: for $m \neq 0$, the unstable region is confined to a narrow strip as η decreases (figure 3), but for $m = 0$ the unstable region remains broad, while migrating to larger Re and larger k (figure 6).

https://doi.org/10.1017/S0022112008002577 Published online by Cambridge University Press

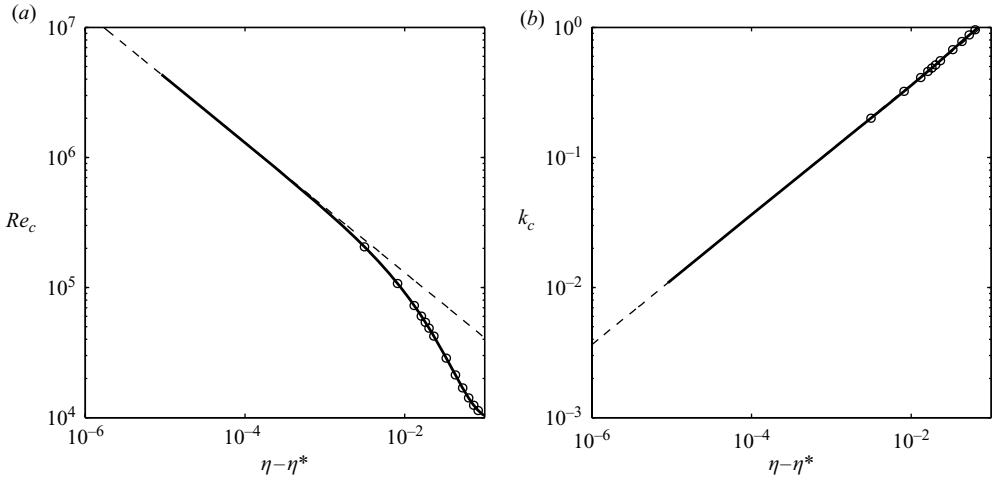


FIGURE 5. For $m=1$, comparison of the asymptotic predictions (3.27)–(3.29) (dashed lines) with numerical data (solid lines and circles): (*a*) critical Reynolds number, (*b*) critical axial wavenumber.

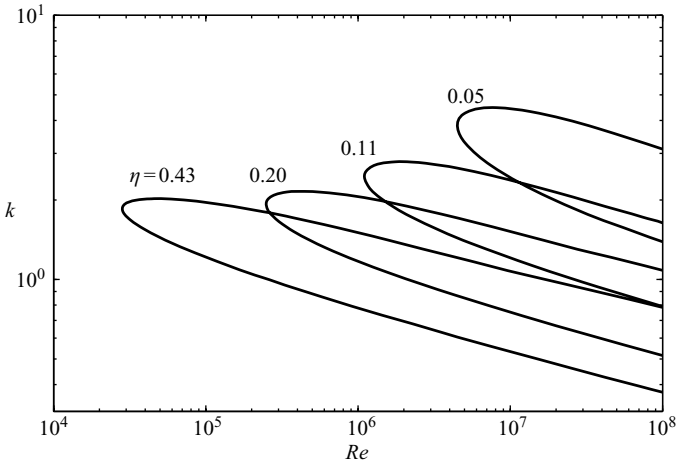


FIGURE 6. Neutral curves for $m=0$ and $\eta=0.43, 0.20, 0.11, 0.05$.

Before commencing our analysis, we note that Mott & Joseph (1968) gave a large-Re approximation to their $m=0$ results in the form of a 'turning-point solution'. The turning-point solution is one of the heuristic methods of approximation reviewed in Drazin & Reid (1981, § 27) and is not strictly asymptotic. Although it is instructive, it cannot give definitive and quantitative information on Re_c. Instead, we wish to attempt an asymptotic analysis based on the limit $\eta \to 0$. The starting point of the analysis is to identify the appropriate scalings of Re_c, k_c and ω_c with η. A detailed inspection of the numerical data for APF with $m=0$ suggests that

$$Re_c = O\left(\frac{\log(\eta^{-1})}{\eta}\right), \quad k_c = O\left(\frac{1}{\eta}\right), \quad \omega_c = O\left(\frac{1}{\eta \log(\eta^{-1})}\right) \tag{4.1}$$

are plausible scalings. Note that the scaling for k_c implies that these are short-wave disturbances. The appearance of $\log(\eta^{-1})$ in (4.1) is not unexpected because of the

https://doi.org/10.1017/S0022112008002577 Published online by Cambridge University Press

form of the mean flow (2.1). The numerical data extend only down to $\eta = 0.0015$, so it is impossible to infer from them the correct dependence on $\log(\eta^{-1})$ with complete certainty. Our strategy will be to propose scalings for Re_c, k_c and ω_c (below), to be confirmed *a posteriori* by comparison to the numerical data.

We now consider the limit $\eta \to 0$ of (2.8), the governing equation for $m = 0$ disturbances. The mean flow (2.1) has the form

$$U(r) = 2\frac{(1-r^2)\log(\eta^{-1}) + \log r}{\log(\eta^{-1}) - 1} + O(\eta) \quad \text{for } r = O(1), \tag{4.2}$$

$$U(R) = 2\frac{\log R}{\log(\eta^{-1}) - 1} + O(\eta/\log(\eta^{-1})) \quad \text{for } R = \frac{r}{\eta} = O(1), \tag{4.3}$$

so there are (at least) two asymptotically distinguished regions to consider. Further, the form of asymptotic expansions of U suggest that we take

$$Re_c = \frac{R_0(\log(\eta^{-1}) - 1)}{\eta}, \quad k_c = \frac{k_0}{\eta}, \quad \omega_c = \frac{\omega_0}{\eta(\log(\eta^{-1}) - 1)}, \tag{4.4}$$

for some constants R_0, k_0 and ω_0. The forms (4.4) are consistent with the orders of magnitude (4.1) inferred from the numerical data, but are expected to be preferable: by using $\log(\eta^{-1}) - 1$ instead of $\log(\eta^{-1})$ we expect the relative error in (4.4) to be $O(\eta)$ instead of $O(1/\log(\eta^{-1}))$.

Consider first the inner region, $R = O(1)$. The leading-order equation in this region is

$$\begin{aligned}(2k_0 \log R - \omega_0)\left(\phi_{RR} - \frac{\phi_R}{R} - k_0^2\phi\right) + \frac{4k_0\phi}{R^2} \\ = \frac{-\mathrm{i}}{R_0}\left[\phi_{RRRR} - \frac{2\phi_{RRR}}{R} + \frac{3\phi_{RR}}{R^2} - \frac{3\phi_R}{R^3} - 2k_0^2\left(\phi_{RR} - \frac{\phi_R}{R}\right) + k_0^4\phi\right].\end{aligned} \tag{4.5}$$

The inner region includes the inner pipe wall at $R = 1$, where the no-slip boundary conditions must be applied. Two more boundary conditions arise from the requirement that the solution of (4.5) matches onto an appropriate solution in the outer region $r = O(1)$. In the outer region, the numerical solutions show strong exponential decay with radius, $\phi \sim \exp(-k_c r)$, so we must have decay as $R \to \infty$ in the inner region. The boundary conditions for (4.5) are therefore:

$$\left.\begin{array}{ll}\phi = \phi_R = 0 & \text{at } R = 1, \\ \phi \to 0 & \text{as } R \to \infty.\end{array}\right\} \tag{4.6}$$

There are two growing and two decaying solutions to (4.5) as $R \to \infty$, so (4.6) constitutes four homogeneous boundary conditions. Together, (4.5) and (4.6) therefore constitute an eigenvalue problem, for example for ω_0 as a function of k_0 and R_0.

Remarkably, the inner region alone determines the leading-order eigenvalue problem. No matching with the outer region is necessary, and the whole of the outer region behaves in a passive manner. A numerical solution of (4.5) and (4.6) is possible using the same pseudospectral collocation technique as described above. When this is done, a neutral curve, on which $\max\{\mathrm{Im}(\omega_0)\} = 0$, is obtained in the (R_0, k_0)-plane. We are interested in the point on this curve with the minimum value of R_0, which is found to be

$$R_0 = 1.3765 \times 10^5, \quad k_0 = 1.6681 \times 10^{-1}, \quad \omega_0 = 2.9262 \times 10^{-2}. \tag{4.7}$$

https://doi.org/10.1017/S0022112008002577 Published online by Cambridge University Press

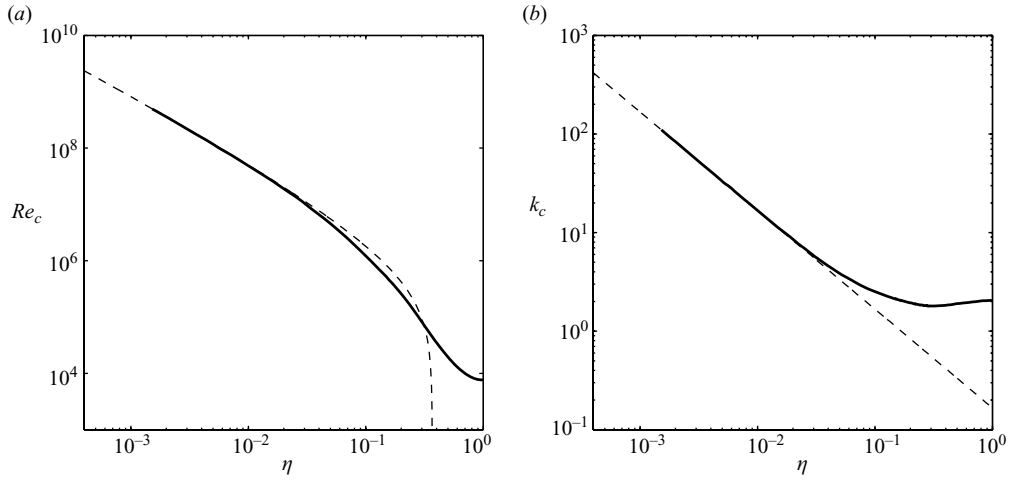


FIGURE 7. For $m = 0$, comparison of the $\eta \to 0$ asymptotic predictions (4.4), (4.7) (dashed lines) with numerical data (solid lines): (*a*) critical Reynolds number, (*b*) critical axial wavenumber.

The asymptotic predictions (4.4) with the values (4.7) are shown in figure 7 by the dashed lines. The agreement with the numerical data is very good, so we conclude that the scalings and analysis given above are a correct description of the axisymmetric instabilities to APF for small η. To complete the description, we note briefly that an analysis of the outer region $r = O(1)$, although not necessary to determine the values (4.7), could be performed: a multiple scales analysis shows that $\phi \sim r^{1/2} \exp(-k_0 r/\eta)$. In order to apply the correct boundary conditions at the outer pipe wall, this in turn must be matched onto a solution in a further region: a thin layer in which $1 - r = O(\eta)$.

5. Discussion

We have investigated the stability properties of annular Poiseuille flow (APF), with particular emphasis on the wide-gap limit in which the radius ratio η is small. We performed numerical calculations of the critical Reynolds number and related quantities in § 2, extending the range of η and Re significantly beyond that considered previously.

We find that the disturbances with $m \neq 0$ display a bifurcation in which $Re_c \to \infty$ and $k_c \to 0$ at a finite critical value of η. This bifurcation is similar to that considered by Cowley & Smith (1985), and was studied asymptotically in § 3. The $m = 0$ disturbances, however, do not follow the same route, and instead they have $Re_c \to \infty$ as $\eta \to 0$, and this process was studied asymptotically in § 4. For both axisymmetric and non-axisymmetric modes there is a good quantitative agreement between the numerical data and the asymptotic predictions, suggesting that the stability characteristics of APF are correctly mapped out.

We conclude that Mott & Joseph (1968) came to the correct conclusion about the stability of APF in the limit $\eta \to 0$, despite the limited range of η they were able to consider (recall the squares in figure 1), and despite their restriction to axisymmetric modes. Consequently, we conclude that Cotrell & Pearlstein (2006) are

https://doi.org/10.1017/S0022112008002577 Published online by Cambridge University Press

incorrect in asserting that APF is stable at all Re for η less than a finite critical value. This is only true of the non-axisymmetric disturbances, and indeed Cotrell & Pearlstein's study correctly discovered the bifurcation of the $m=1$ modes at $\eta \simeq 0.12$.

Some special interest is attached to APF because it connects two important canonical flows: plane Poiseuille flow, as $\eta \to 1$, and Hagen–Poiseuille flow (HPF), as $\eta \to 0$. HPF is recovered point-wise but non-uniformly from APF as $\eta \to 0$, so the interpretation of this limit certainly requires a little care (Mott & Joseph 1968 argue that identifying the limit with HPF is valid because the force per unit length on the inner cylinder tends to zero). In any case, the question of whether APF is stable is itself of practical and academic interest. A consequence of our results is that HPF, long thought (though still without proof) to be stable at all Re, remains an isolated special case instead of being one member of a class of stable annular flows. For the spiral Poiseuille flow studied by Cotrell & Pearlstein this implies that the neutral curve for small values of η has the same topology as for larger η, rather than being qualitatively different. Although this contradicts a conclusion of Cotrell & Pearlstein (2006), we believe that their results for $\eta = 0.1$ are correct over the range of Re they consider ($Re \leqslant 10^5$), and that connection to an axisymmetric Tollmein–Schlichting-like instability would occur at $Re \simeq 10^6$, outside the range of their figures. Concerning the instability modes of small-η APF, we note that they are localized in $r \leqslant O(\eta)$ as $\eta \to 0$ (§ 4), so they disappear in the HPF limit. In a similar vein, HPF with superimposed rigid-body rotation is unstable for arbitrarily slow rotation, with $Re_c \to \infty$ as $\Omega \to 0$ (Stewartson & Brown 1984; Le Dizès & Fabre 2007). The unstable modes in this case are localized in $r \leqslant O(\Omega^{1/2})$ as $\Omega \to 0$, so again they disappear in the HPF limit. Although the stability of HPF is not robust to small flow distortions of these two types (weak swirl or the distortion due to a slender centre body), we note that it is robust to small elliptical deformation of the pipe cross-section (Davey & Salwen 1994; Kerswell & Davey 1996). In fact, fully developed flow in an elliptical pipe is absolutely stable until the aspect ratio exceeds the relatively large value of 10.4 (Kerswell & Davey 1996).

The author is grateful to Dr S. J. Cowley for helpful discussions relating to this work, and to Trinity College Cambridge for its financial support.

Appendix A. The operators L_0, L_1 and L_2

$$L_0 = \begin{pmatrix} \lambda_0^{-1}(c_0\partial_\tau + U\partial_X) & & & & \\ -\partial_y^2 - \phi^{-1}\partial_y + m^2\phi^{-2} & \lambda_0^{-1}U_y & 0 & 0 \\ 0 & (L_0)_{11} + \phi^{-2} & 2\mathrm{i}m\phi^{-2} & \lambda_0^{-1}\partial_y \\ 0 & -2\mathrm{i}m\phi^{-2} & (L_0)_{22} & \lambda_0^{-1}\phi^{-1}\mathrm{i}m \\ \partial_X & \partial_y + \phi^{-1} & \mathrm{i}m\phi^{-1} & 0 \end{pmatrix} \tag{A 1}$$

where

$$\phi = y + \eta^*/(1-\eta^*) \tag{A 2}$$

https://doi.org/10.1017/S0022112008002577 Published online by Cambridge University Press

and subscripts denote partial derivatives in the standard notation.

$$L_1 = \begin{pmatrix} -\lambda_0^{-2}\lambda_1(c_0\partial_\tau + U\partial_X) + \lambda_0^{-1}c_1\partial_\tau & -\lambda_0^{-2}\lambda_1 U_y & 0 & 0 \\ 0 & (L_1)_{11} & 0 & -\lambda_0^{-2}\lambda_1\partial_y \\ 0 & 0 & (L_1)_{11} & -\lambda_0^{-2}\lambda_1\phi^{-1}\mathrm{i}m \\ 0 & 0 & 0 & 0 \end{pmatrix} \tag{A 3}$$

$$L_2 = \begin{pmatrix} \psi(c_0\partial_\tau + U\partial_X) - \lambda_0^{-2}\lambda_1 c_1\partial_\tau + \lambda_0^{-1}(c_2\partial_\tau + \partial_T + U_\eta\partial_X) + \dfrac{(\partial_y - 2m^2\phi^{-1})}{\phi^2(1-\eta^*)^2} - k_s^2\partial_X^2 & \psi U_y + \lambda_0^{-1}U_{\eta,y} & 0 & k_s^2\lambda_0^{-1}\partial_X \\ 0 & -\dfrac{(L_2)_{11}}{2} - \dfrac{-4\mathrm{i}m}{\phi^3(1-\eta^*)^2} & & \psi\partial_y \\ 0 & \dfrac{4\mathrm{i}m}{\phi^3(1-\eta^*)^2} & (L_2)_{22} & -\dfrac{\mathrm{i}m\phi^{-1}\psi}{\lambda_0\phi^2(1-\eta^*)^2} - \dfrac{\mathrm{i}m}{\lambda_0\phi^2(1-\eta^*)^2} \\ 0 & \dfrac{-1}{\phi^2(1-\eta^*)^2} & \dfrac{-\mathrm{i}m}{\phi^2(1-\eta^*)^2} & 0 \end{pmatrix} \tag{A 4}$$

where

$$\psi = \lambda_0^{-3}\left(\lambda_1^2 - \lambda_0\lambda_2\right). \tag{A 5}$$

REFERENCES

Burridge, D. M. & Drazin, P. G. 1969 Comments on 'Stability of pipe Poiseuille flow'. *Phys. Fluids* **12**, 264–265.

Corcos, G. M. & Sellars, J. R. 1959 On the stability of fully developed flow in a pipe. *J. Fluid Mech.* **5**, 97–112.

Cotrell, D. L. & Pearlstein, A. J. 2006 Linear stability of spiral and annular Poiseuille flow for small radius ratio. *J. Fluid Mech.* **547**, 1–20.

Cowley, S. J. & Smith, F. T. 1985 On the stability of Poiseuille–Couette flow: a bifurcation from infinity. *J. Fluid Mech.* **156**, 83–100.

Davey, A. & Salwen, H. 1994 On the stability of flow in an elliptic pipe which is nearly circular. *J. Fluid Mech.* **281**, 357–369.

Drazin, P. G. & Reid, W. H. 1981 *Hydrodynamic Stability*. Cambridge University Press.

Garg, V. K. 1980 Spatial stability of concentric annular flow. *J. Phys. Soc. Japan* **49**, 1577–1583.

Kerswell, R. R. & Davey, A. 1996 On the linear instability of elliptic pipe flow. *J. Fluid Mech.* **316**, 307–324.

Landau, L. D. & Lifshitz, E. M. 1987 *Fluid Mechanics*, 2nd edn. Pergamon.

Le Dizès, S. & Fabre, D. 2007 Large-Reynolds-number asymptotic analysis of viscous centre modes in vortices. *J. Fluid Mech.* **585**, 153–180.

Mahadevan, R. & Lilley, G. M. 1977 The stability of axial flow between concentric cylinders to asymmetric disturbances. *AGARD CP* 224, pp. 9-1–9-10.

https://doi.org/10.1017/S0022112008002577 Published online by Cambridge University Press

Mott, J. E. & Joseph, D. D. 1968 Stability of parallel flow between concentric cylinders. *Phys. Fluids* **11**, 2065–2073.

Schmid, P. J. & Henningson, D. S. 2001 *Stability and Transition in Shear Flows*. Springer.

Smith, F. T. 1979*a* Instability of flow through pipes of general cross-section. Part I. *Mathematika* **26**, 197–210.

Smith, F. T. 1979*b* Instability of flow through pipes of general cross-section. Part II. *Mathematika* **26**, 211–223.

Smith, F. T. & Bodonyi, R. J. 1980 On the stability of the developing flow in a channel or circular pipe. *Q. J. Mech. Appl. Maths* **33**, 293–320.

Smith, F. T. & Bodonyi, R. J. 1982 Amplitude-dependent neutral modes in the Hagen–Poiseuille flow through a circular pipe. *Proc. R. Soc. Lond.* A **384**, 463–489.

Stewartson, K. & Brown, S. N. 1984 Inviscid centre-modes and wall-modes in the stability theory of swirling Poiseuille flow. *IMA J. Appl. Maths* **32**, 311–333.

Walton, A. G. 2005 The linear and nonlinear stability of thread-annular flow. *Phil. Trans. R. Soc. Lond.* **363**, 1223–1233.

https://doi.org/10.1017/S0022112008002577 Published online by Cambridge University Press